Journal of Solid State Chemistry **164,** 210–219 (2002)
doi:10.1006/jssc.2001.9462, available online at http://www.idealibrary.com on IDEAL®

$RuGa_vSn_w$ Nowotny Chimney Ladder Phases and the 14-Electron Rule

Guoxin Lu,* Stephen Lee,*,†,[1] Jianhua Lin,*,[1] Liping You,‡ Junliang Sun,* and Joshua Teal Schmidt†

*State Key Laboratory for Rare Earth Chemistry and Applications, College of Chemistry and Molecular Engineering, Peking University, Beijing, 100871, China; †Department of Chemistry and Chemical Biology, Baker Laboratory, Cornell University, Ithaca, New York 14853-1301; and ‡Laboratory of Electron Microscopy, Department of Physics, Peking University, Beijing, 100871, China
E-mail: sl137@cornell.edu

Received August 16, 2001; in revised form October 29, 2001; accepted November 16, 2001

A series of ruthenium gallium stannides have been prepared with stoichiometry $RuGa_vSn_w$, where $8+3v+4w=14$ and $0 < v < 0.70$. These samples have been analyzed by X-ray powder diffraction and transmission electron microscopy (TEM). The data show that these compounds are Nowotny chimney ladder phases with both commensurate and incommensurate structures. We show that there are special characteristics in chimney ladder powder diffraction patterns that allow one to determine the ratio of main group atom-sites to transition metal atom-sites to high accuracy. Our results confirm earlier work which suggest that both the stoichiometry and the structure of chimney ladder phases are dominated by electronic factors. The structures reported in this paper adhere to the 14-electron rule, i.e., there are 14 valence electrons per transition metal ion. The interplay of main group and transition metal structures leads to a pseudo *c*-axis, the presence of which is confirmed by the TEM data. We discuss the relation between these phases and the Fibonacci sequence. © 2002 Elsevier Science (USA)

INTRODUCTION

Incommensurate crystal structures are fairly common. Among the best understood are those with charge density waves (CDW) (1, 2). In such systems, the atoms in the crystal are displaced from an idealized and generally small unit cell in a fashion incommensurate with this original unit cell. An elegant theory that explains much about these systems has been developed (3). In this theory one focuses on the shape of the Fermi surface of the original small unit cell. It is generally found that the reciprocal lattice vector that maximally maps the Fermi surface onto itself is the experimentally observed incommensurate reciprocal lattice vector.

The situation is much less satisfactory for other types of incommensurate systems. Chief among these are those with matter occupation waves (MOW). In such systems, also called Vernier systems (4, 5), there are generally at least two atom types. Each type is in a simple ordered array, but the two arrays are not commensurate with each other. In some cases this lack of commensurability is related to the relative size of the atoms. In other cases electronic rather than steric factors are more important (6). These latter electronic phases are particularly troublesome, for although one suspects that the Fermi surface is responsible for the observed superstructures, because there is no single simple undistorted unit cell, one can not directly apply the previously developed principle of maximal Fermi surface interaction.

An extensive MOW family where electronic factors predominate are the Nowotny chimney ladder phases (7–36). These compounds are generally tetragonal and are composed of two separate sublattices. The first is a tetragonal array of transition metal atoms, generally from groups 4 through 9 of the periodic table. Contained within this array of transition metal atoms is a second network of main group atoms, typically from group 13 or group 14. The mismatch between these two networks can lead to large superstructures or even incommensurate phases. Among the simplest commensurate systems are the Mn_4Si_7, Ru_2Ge_3, Ir_3Ga_5, and Ir_4Ge_5 structures. However, more complex commensurate structures have also been reported: $V_{17}Ge_{31}$, $Cr_{11}Ge_{19}$, $Mn_{11}Si_{19}$, $Mn_{15}Si_{26}$, Mo_9Ge_{16}, $Mo_{13}Ge_{23}$, $Rh_{10}Ga_{17}$, and $Rh_{17}Ge_{22}$.

Particularly interesting for the understanding of these structures is the observation by Jeitschko, *et al.* (18, 28) that Nowotny chimney ladder phases follow an electron counting rule. Phases where the transition element is a group 5 metal have 12 valence electrons per transition metal atom (e^-/T), those with a group 6 metal have 13 e^-/T, while group 7 through 9 transition elements have 14 e^-/T. Thus Mn_4Si_7, Ru_2Ge_3, and Ir_4Ge_5 all have 14 e^-/T.

Almost all binary chimney ladder phases are tetralides. Ternary systems containing trilides however are also known. For these latter systems it is convenient to formally

[1] To whom correspondence should be addressed.

0022-4596/02 $35.00

transfer one valence electron from the transition metal to each of the trilide atoms, making the trilide isoelectronic with the tetralide. For example, in Ir_3Ga_5, which is one of only three known trilide binary chimney ladder phases, after such an electron transfer there are only 7.33 valence electrons remaining on the T atom ($7.33 = 9 - 5/3$). We will call 7.33 the corrected T group number for this system. This corrected T group number is related to e^-/T but, unlike e^-/T, retains direct information of the original T group number. It is useful as the chimney ladder electron counting rule depends explicitly on the transition metal group number.

In Fig. 1 we compare the corrected transition metal group number (abbreviated hereafter as corrected T) with e^-/T for all known systems where the corrected T is greater than 6.5. For corrected T values ranging from 6.5 to 7.25, there is an excellent correlation between corrected T and e^-/T. However for corrected T values above 7.25, there is a much greater dispersion in the reported structures. While according to Jeitschko *et al.*'s rule the value of e^-/T should remain constant at 14.0 e^-/T; in practice, values as low as 13.87 and as high as 14.22 are observed. Some of this latter dispersion is real, but it should be recalled that e^-/T is determined from the atomic composition. For intermetallic systems, exact knowledge of atomic composition is difficult to obtain. Generally the best method of elemental analysis is through electron microprobe, a method that can have substantial numerical errors.

In this paper we report on a new family of Nowotny chimney ladder phases, ruthenium gallium stannides. Our focus is on the precision of the 14-electron rule. We therefore prepared a series of compounds $RuGa_vSn_w$ where v and w are subject to the constraint $8 + 3v + 4w = 14$. As Ru, Ga, and Sn have respectively 8, 3, and 4 valence electrons the compounds are constrained to have exactly 14 e^-/T.

By X-ray powder analysis, we find single-phase products for values of v, $0 \leq v \leq 0.70$. Across this range of x values, one finds a continuous series of commensurate and incommensurate phases. This incommensurability proves important with respect to the 14-e^-/T rule. For, as we shall show below, the incommensurability allows the refinement of the parameter, $v + w$. As is well known, powder diffraction can be used to determined lattice parameters to exquisite accuracy. In exactly the same manner, we can determine $v + w$ to great accuracy. However as $v + w$ relates to stoichiometry, we can therefore internally verify the phase purity with high accuracy and hence the value of e^-/T. With this internal corroboration in hand, we conclude that the 14-e^-/T rule is extremely well behaved for these $RuGa_vSn_w$ systems, with deviations an order of magnitude less than that for ternary systems previously reported.

This is a useful finding. It demonstrates the preeminent role electronic factors play in Nowotny chimney ladder structures. Finally, we examine the $RuGa_vSn_w$ phases by electron diffraction. Not only do the electron diffraction results confirm the analysis based on powder diffraction, they show clearly that in addition to the 14-e^-/T rule, there is also a further structural relation between the transition metal and main group atomic positions. As will be described below, this further relation is again expressible in terms of the stoichiometric ratio of the transition metal to the main group atoms.

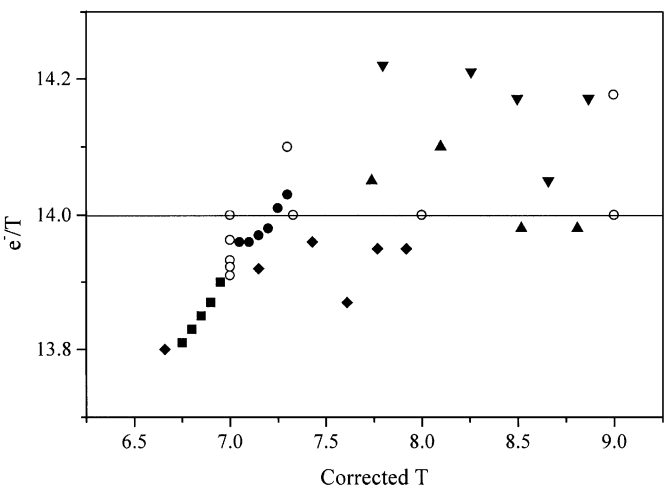

FIG. 1. Number of valence electrons per atom (e^-/T) as a function of the corrected transition metal group number for all known later transition metal element Nowotny chimney ladder phases. One compound, Co_2Si_3, has been omitted from this graph as its e^-/T value of 15.0 is off-scale with respect to all other known phases. ■, Mn–Cr–Si; ●, Mn–Fe–Si; ▲, Ir–Ga–Ge; ▼, Rh–Ga–Ge; ◆, Ru–Ga–Ge; ○, binary.

EXPERIMENTAL METHODS

Samples of the Ru–Ga–Sn ternary system were prepared by the following method. Ruthenium powder (purity 99.95%, Alfa Aesar Company), tin powder (purity 99.5%, Wuhan Xin'ao Chemical Company), and gallium ingots (purity 99.999%, Shanghai Chemical Reagent Company) were vacuum sealed in quartz tubes. The samples were then placed in muffle furnaces, gradually heated at a rate of 2°C/min to 950°C, and annealed at this temperature for 100 h. All samples were initially cooled at the rate of 0.5°C/min. In the case of $RuGa_{0.061}Sn_{1.440}$, $RuGa_{0.400}Sn_{1.200}$, $RuGa_{0.472}Sn_{1.147}$, and $RuGa_{0.719}Sn_{0.963}$ once the temperature of 400°C was reached, the samples were quenched to room temperature with water. In the remaining samples, the cooling rate of 0.5°C/min was maintained until room temperature. In the former case, small amounts of Ru_3Sn_7 were observed in the powder diffraction patterns. In the latter case no Ru_3Sn_7 could be detected by powder methods. In all samples, however, the amount of Ru_3Sn_7 could be estimated from the powder data to be 1% or less of the total sample mass.

Powder X-ray diffraction data were made on a Rigaku D/max-2000 X-ray diffractometer with Cu$K\alpha$ radiation. The raw data were analyzed by PowderX (37). For commensurate cell refinement, the program Finax was used; incommensurate refinement was based on a set of programs adapted from Lazy-Pulverix (38). Electron diffraction studies were carried out on a Hitachi H-90000 electron microscope. A rotational goniometric specimen stage was used in the electron diffraction studies, so that the angle between the axes of the observation zones could be monitored with reasonable accuracy.

RESULTS

Nowotny chimney ladder structures consist of two separate sublattices. The transition metal atoms form by themselves the tetragonal β-Sn structure. The main group atoms are then arrayed in helices in the interstices of this transition metal β-Sn-type lattice. An example of such a structure is Ru_2Sn_3: it is illustrated in Fig. 2.

Indexation of X-ray powder data and indeed the identification of new Nowotny chimney ladder phases are greatly facilitated by special characteristics of chimney ladder diffraction patterns. In Fig. 3 we illustrate the powder patterns of two known chimney ladder compounds, $Rh_{17}Ge_{22}$ and $Mo_{13}Ge_{23}$. In both, there are several intense peaks with Cu$K\alpha$ 2θ positions between 25° and 55°. The indexed names of these reflections are also given in the figure. It may be seen that there is a correspondence with the names of these reflections and the stoichiometry of the compounds. If we consider T_tM_m, where T and M refer to the transition metal and main group atoms and t and m are the respective stoichiometries, then in both cases the principal reflections are (2 1t), (1 1 2t), (2 2 0), (2 1$m - t$), (1 1m), (3 0t), and (1 0t).

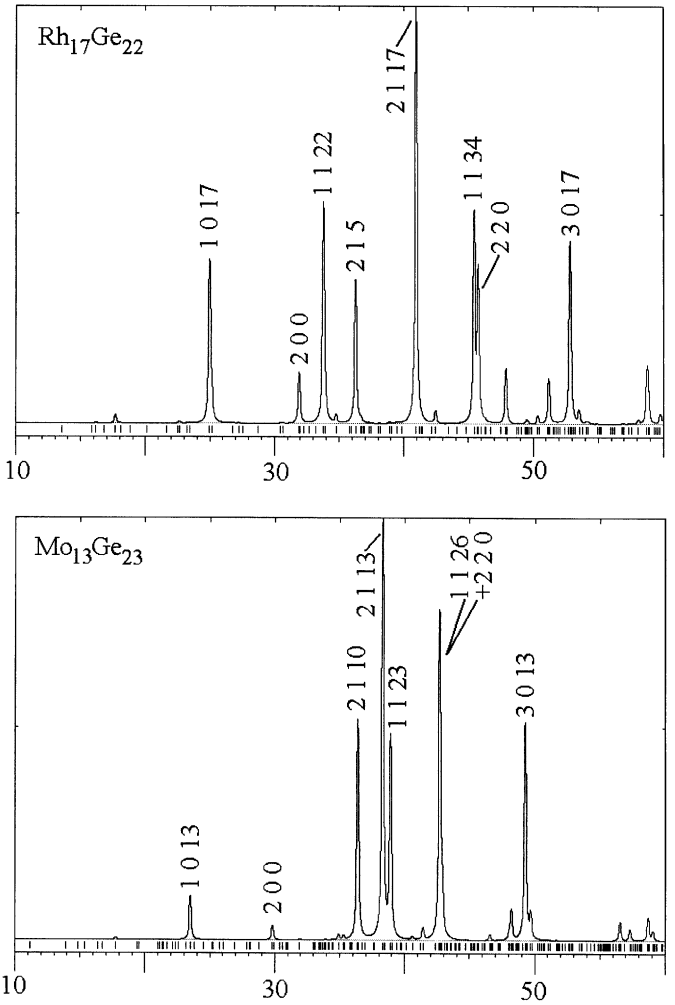

FIG. 3. Calculated powder patterns for the two chimney ladder phases, $Rh_{17}Ge_{22}$ and $Mo_{13}Ge_{23}$.

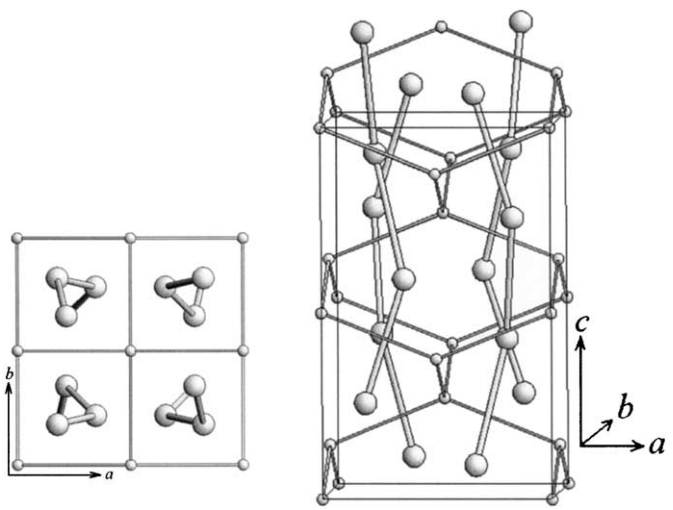

FIG. 2. The crystal structure of Ru_2Sn_3, a representative chimney ladder phase. Smaller spheres, Ru, larger spheres, Sn.

These reflections are the dominant reflections in all known chimney ladder phases.

In indexing any new potential chimney ladder phase, one therefore seeks first to identify these seven dominant reflections. Several of these peaks appear in only a narrow range of values: for example, (2 1t) is always located between 37° and 44° (Cu$K\alpha$ radiation), while (2 2 0) is found between 41° and 49°. It is best to first concentrate on the five reflections (2 1t), (2 2 0), (1 1 2t), (3 0t), and (1 0t), as these five reflections have no m dependence and therefore can be determined without optimization of any parameter (as no value of m is chosen, the actual value chosen for t is at this point immaterial). Only once a valid assignment for these five reflections is found do we turn to the (2 1$m - t$) and (1 1m) reflections. In particular, we choose the values of m and t which lead to the best fit for these latter two reflections.

At this point we turn to higher angle reflections. Higher angle peaks often include (3 1m), (3 2t), (3 1 2$m - 2t$), (1 0 3t),

$(3\ 2\ 2m-t)$, $(4\ 0\ 0)$, $(2\ 1\ m+t)$, $(2\ 1\ 2m-t)$, $(3\ 1\ 2t)$, $(3\ 2\ 3m-3t)$, $(0\ 0\ 2m)$, $(2\ 1\ 3t)$, $(3\ 0\ 2m-t)$, $(4\ 1t)$, $(4\ 0\ 2m-2t)$, $(4\ 2\ 0)$, $(2\ 2\ 2m)$, $(2\ 0\ 2m)$, $(3\ 3\ 2m-2t)$, $(0\ 0\ 4t)$, $(3\ 3\ 2t)$, and $(4\ 2\ 2m-2t)$. If the powder pattern in question is a true chimney ladder phase, we expect to see many of these additional reflections. Furthermore, as the values of t and m have been determined by the first set of seven reflections, there are no additional undetermined parameters. The existence of these latter reflections is therefore an efficient test for a chimney ladder phase.

We have applied this method to $RuGa_vSn_w$ $(0 < v < 0.70)$ systems. In Table 1 we show a sample indexation for a system with an initial loaded composition of $RuGa_{0.200}Sn_{1.350}$. All seven of the first set of reflections described above were observed. Of the second set of 22 commonly observed higher angle reflections, 15 were unambiguously assigned. As Table 1 shows, errors between calculated and observed 2θ positions are generally less than 0.02°, and in no case larger than 0.03°. We conclude that this $RuGe_{0.200}Sn_{1.350}$ system forms a chimney ladder phase. If one chooses a commensurate cell, values for t and m are respectively 20 and 31.

In exactly the same manner we may index other $RuGe_vSn_w$ systems. These additional cell indexations are given in the supplementary material. In each case, the errors between calculated and observed 2θ positions are small (generally less than 0.02°), indicating the validity of the proposed cell. In Table 2 we list a commensurate cell which gives optimal or near optimal agreement between observed and calculated diffraction angles. In Fig. 4 we show a series of these powder patterns for the $RuGa_vSn_w$ $(0 < v < 0.70)$ system. As can be seen in this figure, the powder patterns evolve continuously in this region. Peaks that have only t indices are relatively unchanged, while those that depend primarily on m shift in a substantial way. For example, the $(11m)$ peak shifts from 37° to 34° in 2θ, a shift in d-spacing of 0.21 Å.

We may use this continuous evolution of the powder patterns to finish the powder pattern indexation. Examination of the powder data allows us to correlate peaks in one powder pattern with those with adjacent stoichiometries. In this way we are able to assign the $(1\ 1\ 2m-2t)$, $(2\ 0\ 2m-2t)$, $(1\ 0\ 2m-t)$, $(2\ 2\ 2t-m)$, $(2\ 0\ 2t)$, $(3\ 1\ 2t-m)$, $(4\ 1m-t)$, $(3\ 2\ 2m-t)$, $(4\ 2\ 2t-m)$, $(4\ 0\ 2t)$, $(3\ 2m+t)$, $(3\ 0\ 3t)$, $(4\ 3\ 2m-3t)$, $(2\ 1\ 3m-t)$, $(4\ 3m-t)$, $(5\ 1\ 2t-m)$, $(4\ 3t)$, $(3\ 2\ 3t)$, $(4\ 1m+t)$, $(2\ 2\ 2t+m)$, $(2\ 0\ 4t)$, $(5\ 1m)$, $(5\ 2t)$, $(4\ 1\ 3t)$, $(5\ 1\ 2t)$, $(2\ 2\ 4t)$, $(1\ 1\ 3m)$, $(6\ 0\ 0)$, $(5\ 2\ 3t-m)$, and $(5\ 3\ 2m-2t)$ peaks. The cell parameters reported in Table 2 are based on least-squares refinements, which include these additional reflections. We report in Table 2 the initial loaded stoichiometries, the ratio of main group to transition metal atoms loaded in the samples, optimal values for m and t, the a and c lattice constants, and finally c_{pseudo}, c_m, and c_t where $c_{\text{pseudo}} = c/(2t-m)$, $c_m = c/m$, and $c_t = c/t$. These final three lattice constants are related to the sublattice constants for respectively the transition metal and main group sublattices. The parameter c_{pseudo} is particularly useful in accounting for the electron diffraction data that will be discussed later.

TABLE 1
Powder Refinement for $RuGa_{0.200}Sn_{1.350}$

Intensity	2θ (calc.)	2θ (obs.)	Index (hkl)	HKL
5.31	23.07	23.06	1 0 20	$1\ 0\ t$
1.49	28.53	28.51	1 1 22	$1\ 1\ 2m-2t$
61.08	33.99	33.99	2 1 11	$2\ 1\ m-t$
74.16	34.87	34.86	1 1 31	$1\ 1\ m$
3.79	35.30	35.28	2 0 22	$2\ 0\ 2m-2t$
100.00	37.33	37.34	2 1 20	$2\ 1\ t$
8.47	41.07	41.07	1 0 42	$1\ 0\ 2m-t$
35.24	41.39	41.40	2 2 0	2 2 0
34.28	42.04	42.05	1 1 40	$1\ 1\ 2t$
10.85	42.24	42.23	2 2 9	$2\ 2\ 2t-m$
2.76	47.14	47.16	2 0 40	$2\ 0\ 2t$
8.11	47.32	47.32	3 1 9	$3\ 1\ 2t-m$
52.86	47.91	47.91	3 0 20	$3\ 0\ t$
6.22	51.03	51.03	3 1 22	$3\ 1\ 2m-2t$
5.11	54.59	54.59	3 2 11	$3\ 2\ m-t$
3.29	55.20	55.19	3 1 31	$3\ 1\ m$
5.51	57.88	57.91	0 0 62	$0\ 0\ 2m$
5.64	57.98	57.98	1 0 60	$1\ 0\ 3t$
13.55	58.20	58.20	2 1 51	$2\ 1\ m+t$
5.56	59.73	59.73	3 0 42	$3\ 0\ 2m-t$
3.74	59.97	59.98	4 0 0	4 0 0
7.17	60.47	60.49	3 1 40	$3\ 1\ 2t$
9.14	62.96	62.96	4 1 11	$4\ 1\ m-t$
2.97	63.80	63.81	4 0 22	$4\ 0\ 2m-2t$
4.73	65.13	65.13	4 1 20	$4\ 1\ t$
8.97	66.00	66.01	2 0 62	$2\ 0\ 2m$
8.99	67.71	67.71	3 2 42	$3\ 2\ 2m-t$
12.64	67.94	67.94	4 2 0	4 2 0
6.80	68.55	68.54	4 2 9	$4\ 2\ 2t-m$
1.78	71.54	71.54	4 2 22	$4\ 2\ 2m-2t$
3.03	72.21	72.22	4 0 40	$4\ 0\ 2t$
5.05	73.71	73.72	3 0 60	$3\ 0\ 3t$
2.80	73.90	73.90	3 2 51	$3\ 2\ m+t$
15.29	75.93	75.94	3 3 40	$3\ 3\ 2t$
1.24	78.18	78.18	4 3 11	$4\ 3\ m-t$
2.60	78.77	78.78	2 1 73	$2\ 1\ 3m-t$
3.23	79.72	79.70	5 1 9	$5\ 1\ 2t-m$
6.85	80.17	80.17	4 3 20	$4\ 3\ t$
4.95	81.05	81.06	3 2 60	$3\ 2\ 3t$
5.40	81.23	81.24	4 1 51	$4\ 1\ m+t$
1.39	82.18	82.17	2 2 71	$2\ 2\ 2t+m$
2.56	84.53	84.53	2 0 80	$2\ 0\ 4t$
2.66	85.91	85.90	5 1 31	$5\ 1\ m$
6.44	87.37	87.37	5 2 20	$5\ 2\ t$
6.17	88.24	88.25	4 1 60	$4\ 1\ 3t$
10.62	90.38	90.39	5 1 40	$5\ 1\ 2t$
3.65	91.69	91.69	2 2 80	$2\ 2\ 4t$
1.78	92.18	92.17	5 2 33	$5\ 2\ 3m-3t$
2.10	96.67	96.65	1 1 93	$1\ 1\ 3m$
2.92	96.91	96.91	5 3 22	$5\ 3\ 2m-2t$
4.04	97.12	97.12	6 0 0	6 0 0

TABLE 2
Refined Cell Parameters for $RuGa_vSn_w$ Samples

Loaded stoichiometry	$y = \frac{[Ga]+[Sn]}{[Ru]}$	t^a	m^a	m/t^a	m/t^b	a [Å]	c [Å]	$c_t = c/t$ [Å]	$c_m = c/m$ [Å]	$c_{pseudo} = c/(2t - m)$ [Å]	Corr. T
$RuSn_{1.5}$	1.4994	2	3	1.5000	1.5000	6.1789(3)	9.9227(6)	4.9614(3)	3.3076(2)	9.9227(6)	8.000
$RuGa_{0.061}Sn_{1.440}$	1.5165	21	32	1.5244	1.5238	6.1834(2)	104.004(5)	4.9526(2)	3.2501(2)	10.4004(5)	7.939
$RuGa_{0.081}Sn_{1.438}$	1.5186	19	29	1.5267	1.5268	6.1811(2)	94.029(5)	4.9489(3)	3.2423(2)	10.4476(5)	7.919
$RuGa_{0.160}Sn_{1.382}$	1.5423	11	17	1.5456	1.5444	6.1726(3)	54.354(4)	4.9413(4)	3.1973(2)	10.8708(8)	7.840
$RuGa_{0.200}Sn_{1.350}$	1.5495	20	31	1.5504	1.5495	6.1703(2)	98.772(4)	4.9386(2)	3.1862(1)	10.9746(4)	7.800
$RuGa_{0.240}Sn_{1.319}$	1.5588	25	39	1.5601	1.5595	6.1641(2)	123.353(6)	4.9341(2)	3.1629(1)	11.2148(5)	7.760
$RuGa_{0.320}Sn_{1.259}$	1.5789	19	30	1.5798	1.5800	6.1517(3)	93.558(7)	4.9241(4)	3.1196(2)	11.6947(4)	7.680
$RuGa_{0.400}Sn_{1.200}$	1.6000	5	8	1.6000	1.6000	6.1392(2)	24.604(1)	4.9208(2)	3.0755(1)	12.3020(5)	7.600
$RuGa_{0.461}Sn_{1.156}$	1.6167	13	21	1.6155	1.6154	6.1299(2)	63.944(3)	4.9188(2)	3.0450(1)	12.7889(5)	7.539
$RuGa_{0.482}Sn_{1.137}$	1.6181	55	89	1.6181	1.6179	6.1264(2)	270.47(2)	4.9176(4)	3.0390(3)	12.8795(9)	7.518
$RuGa_{0.472}Sn_{1.147}$	1.6187	34	55	1.6181	1.6169	6.1288(2)	167.248(10)	4.9191(3)	3.0409(2)	12.8652(8)	7.528
$RuGa_{0.499}Sn_{1.122}$	1.6202	8	13	1.6260	1.6238	6.1215(3)	39.330(3)	4.9163(4)	3.0254(2)	13.1100(10)	7.501
$RuGa_{0.559}Sn_{1.080}$	1.6386	36	59	1.6393	1.6377	6.1159(2)	177.070(11)	4.9186(4)	3.0012(2)	13.6208(8)	7.441
$RuGa_{0.640}Sn_{1.018}$	1.6579	26	43	1.6529	1.6542	6.1040(1)	127.730(5)	4.9127(2)	2.9705(1)	14.1922(5)	7.360
$RuGa_{0.642}Sn_{1.019}$	1.6586	35	58	1.6584	1.6563	6.1035(2)	171.967(10)	4.9133(3)	2.9649(2)	14.3306(8)	7.358
$RuGa_{0.719}Sn_{0.963}$	1.6814	31	52	1.6774	1.6774	6.0922(2)	152.153(7)	4.9082(2)	2.9260(1)	15.2153(7)	
$RuGa_{0.880}Sn_{0.842}$	1.7216	10	17	1.7007	1.7000	6.0843(1)	49.044(2)	4.9044(2)	2.8849(1)	16.3480(7)	
$RuGa_{0.958}Sn_{0.779}$	1.7366	27	46	1.7036	1.7024	6.0857(3)	132.418(10)	4.9044(4)	2.8787(2)	16.5523(12)	
$RuGa_{1.204}Sn_{0.601}$	1.8048	37	63	1.7036		6.0841(2)	181.419(11)	4.9032(3)	2.8797(2)	16.4926(10)	
$RuGa_{1.600}Sn_{0.300}$	1.8974	41	70	1.7065		6.0857(4)	201.21(3)	4.9076(7)	2.8744(4)	16.7676(25)	
$RuGa_{1.795}Sn_{0.150}$	1.9441	17	29	1.7065		6.0867(4)	83.392(9)	4.9054(5)	2.8756(3)	16.6784(18)	

[a] Commensurate refinement.
[b] Incommensurate refinement.

Up to now, we have discussed only commensurate refinements of the lattice constants. We now turn to incommensurate refinements. In this approach we refine the two subcell lattices (i.e., the lattice that describes the transition metal β-Sn framework, and the lattice that describes the main group helical structure) independent of one another. In an incommensurate refinement we no longer require that there is a rational-number-ratio between the axis parameters of these two lattices: the β-Sn sublattice can have a lattice constant, and the main group helix may have *any* other lattice constant.

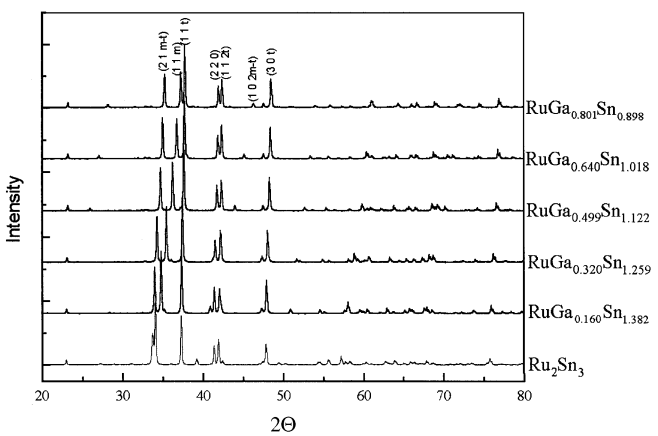

FIG. 4. Representative series of powder patterns for $RuGa_vSn_w$ ($0 \le v \le 0.70$ and $8 + 3v + 4w = 14$). The indices m and t are refinable parameters and also refer to the number of main group atoms (m) and transition metal atom (t) sites in the unit cell.

Some thought will show that such an incommensurate refinement does not require a special computer algorithm. Instead it is straightforward to adapt standard commensurate powder indexation programs for this purpose. One does so in the following manner.

As described above, for each set of data, we have identified 30–40 common reflections. For each of them, we know their indexation with respect to both m and t. In a commensurate refinement m and t must both be integers. In an incommensurate refinement m and t need not be so. We now consider values of m and t ranging from 1 to 1000. For each particular value of m and t, we calculate the standard deviation in the refined value of the a and c lattice constants. In Fig. 5 we plot the ratio of the standard deviation in the a and c lattice constants divided by respectively the a and c lattice parameters, as a function of the ratio of m and t. The results shown in Fig. 5 are for the sample with initial composition $RuGa_{0.320}Sn_{1.259}$. However, all samples show rather similar curves. In each case, the ratio of the standard deviation in the axes to the axes lengths themselves is a smooth function of the ratio of m and t. For both the a and c axes, there is a single minimum, and this minimum occurs

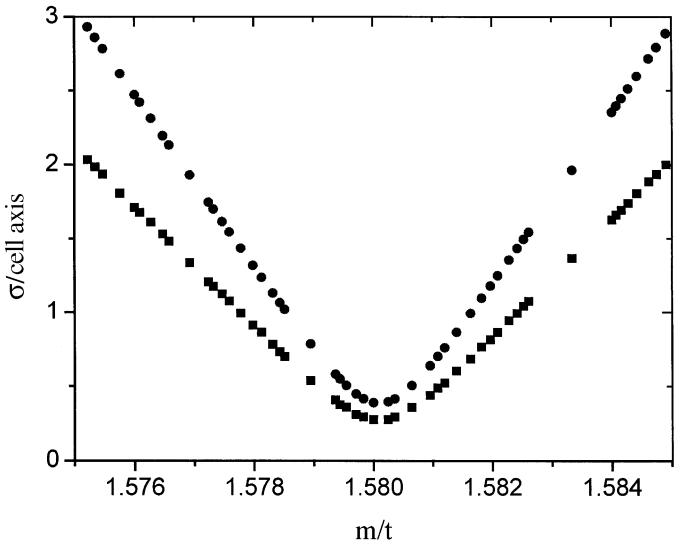

FIG. 5. σ_a/a (■) and σ_c/c (●) as a function of m/t. The minima in these curves correspond to the optimal incommensurate refinement of m/T.

at the same m/t ratio. It is evident that the minimum of this curve corresponds to the optimal incommensurate cell. In Table 2 we compare the values of m/t for both the commensurate and incommensurate refinements. It may be seen that the values are substantially the same. In some cases, such as found for the samples with initial loaded compositions of $RuGa_{0.400}Sn_{1.200}$ and $RuGa_{0.499}Sn_{1.122}$, the values of m and t are so small that a commensurate cell seems likely. In other cases, the values of m and t are sufficiently large that an incommensurate cell is plausible.

Particular attention should be paid to the system whose values of m and t are smallest. They are the two binary compounds, $RuGa_2$ and Ru_2Sn_3, as well as the ternary compounds $RuGa_{0.400}Sn_{1.200}$ and $RuGa_{0.499}Sn_{1.122}$. In these four cases the ratios of t:m are 1:2, 2:3, 5:8, and 8:13. These values are of particular interest for their relation with the Fibonacci sequence.

We recall that the Fibonacci sequence begins 1, 1, 2, 3, 5, 8, 13, …, every number being the sum of the two previous numbers. The relation between this sequence and the four stoichiometries with m:t ratios of 2:1, 3:2, 8:5, and 13:8 is clear. In all cases, the ratios involve two adjacent members of the Fibonacci sequence. The only stoichiometry missing is 5:3. At this point the main interest here is that the ruthenium gallium stannide chimney ladder phases may be used to create structures that correspond to the Fibonacci sequence, a sequence known to be important in quasicrystals (39). However, please note, our data do not suggest any added stability conferred to the phases corresponding to this sequence. Our data are perfectly compatible with ruthenium gallium stannides forming a solid solution with respect to gallium and tin substitutions.

We now turn to the relation between m and t and putative stoichiometry. As described above, m and t are parameters deduced from powder pattern refinement. They are also, however, proportional to the number of main group and transition metal atom sites in the actual crystal structure. However, as in all chimney ladder phases studied by single-crystal methods we know of, there are no examples where atomic site positions are not fully occupied, nor any examples where there is substitutional disorder of main group atoms in transition metal sites; thus, we may expect the number of sites to correspond directly to the number of atoms. In Fig. 6 we therefore compare the values of m/t with the loaded stoichiometry of main group atoms to transition metal atoms, ([Ga] + [Sn])/[Ru].

In this figure, we differentiate the samples in which the only chimney ladder phase observed is a ternary ruthenium gallium stannide from those where in addition the chimney ladder phase $RuGa_2$ is also present. As Fig. 6 shows, the two sets of data are quite distinct from each other. Where no $RuGa_2$ was detected, there is a homogeneous linear correlation between m/t and ([Ga] + [Sn])/[Ru]. By contrast, when $RuGa_2$ is present, m/t depends very little on the loaded main group to transition metal stoichiometry. This evolution from a single-phase region to a two-phase region is further supported by a plot of cell parameters, a and c_m as a function of ([Ga] + [Sn])/[Ru] (see Fig. 7). For values of the m/t parameter between 1.50 and 1.70, there is a steady decrease in a and c_m. For ratios of main group to transition metal above 1.70, no such evolution of lattice constants is seen.

Of particular interest is the single-phase region found for $1.50 \leq m/t \leq 1.70$. Shown in Fig. 6 is the line with unit slope.

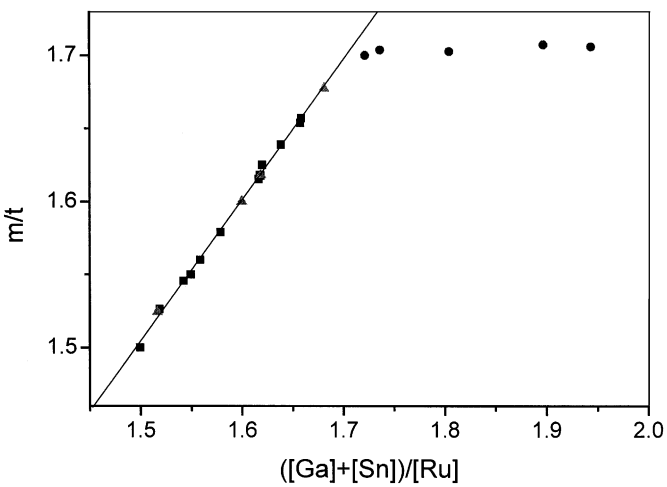

FIG. 6. m/t as a function of initially loaded ([Ga] + [Sn])/[Ru] stiochiometry. Squares refer to samples where no known binary Ru–Sn, Ru–Ga, or Ga–Sn compounds were observed in the powder data. Circles refer to compositions where $RuGa_2$ was observed and triangles to samples containing Ru_3Sn_7. (See Experimental Methods for discussion of Ru_3Sn_7.) The line corresponds to the homogeneous line with unit slope.

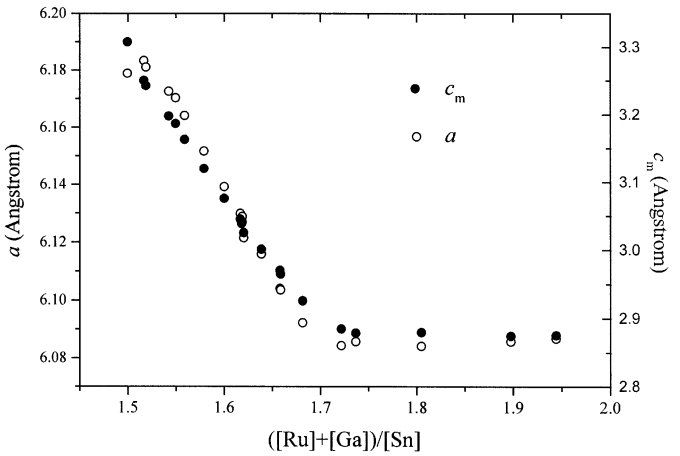

FIG. 7. The cell parameters a and c_m as a function of the initially loaded ([Ga] + [Sn])/[Ru] stiochiometry.

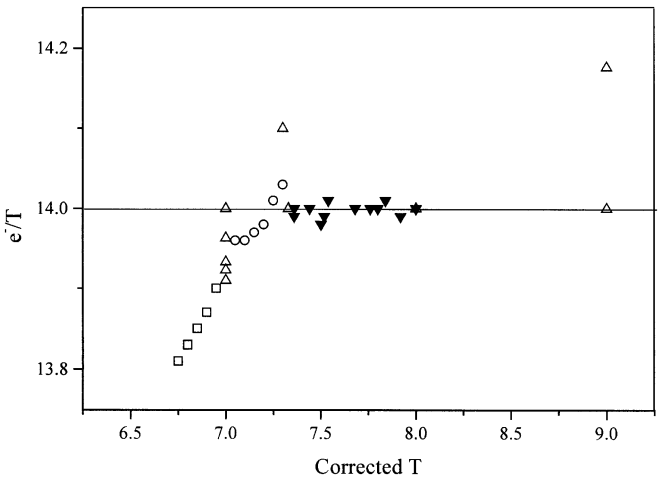

FIG. 8. e^-/T as a function of corrected T group number for the known binary (△), Mn–Cr–Si, (□), Mn–Fe–Si (○), and Ru–Ga–Sn (▼) systems. One compound, Co_2Si_3, has been omitted from this graph as its e^-/T value of 15.0 is off-scale with respect to all other known phases.

As may be seen, there is excellent agreement between this line and the actual data. In other words, the loaded sample stoichiometric ratio between main group and transition metal atoms is always nearly equal to the main group to transition metal ratios derived from the powder pattern indexation. This high degree of correlation suggests that the stoichiometric ratio loaded in the tube is essentially the stoichiometric ratio in the final product.

In summary, in analyzing the powder data for m/t between 1.50 and 1.70, we have found only a single ruthenium-gallium-stannide phase. The unit cell in this region evolves in a characteristic manner. Furthermore due to the special characteristics of chimney ladder diffraction patterns we are able to use powder pattern indexation to confirm the actual stoichiometry of the observed diffracting phase. We conclude that for $RuGa_vSn_w$ where $8 + 3v + 4w = 14$ and where $1.50 < m/t < 1.70$, the samples form in essentially quantitative and pure fashion.

In Fig. 8, we consider again the corrected T group number. We plot the relation between the corrected group T number for all literature binary phases, the literature ternary systems, manganese chromium silicides, and manganese iron silicide vs the number of valence electrons per transition metal (e^-/T). Also included in this figure are the newly acquired data for ruthenium gallium stannides. The data in this figure are in contrast to the earlier picture shown in Fig. 1. It seems that for the three ternary systems shown in Fig. 7, there is a direct correlation between corrected T and e^-/T. Above a corrected $T = 7.0$ to 7.25, e^-/T is constantly at 14.0 e^-/T. Below this value there is a nearly linear decrease in e^-/T as a function of corrected T.

ELECTRON DIFFRACTION

While we were unable to prepare samples suitable for single-crystal X-ray analysis, we were able to study $RuGa_vSn_w$ phases by electron diffraction. Shown in Fig. 9 are electron diffraction images obtained for $RuGa_{0.200}Sn_{1.350}$, $RuGa_{0.320}Sn_{1.260}$, $RuGa_{0.400}Sn_{1.200}$, and $RuGa_{0.499}Sn_{1.122}$. In Fig. 9, all the images are taken normal to the [110] direction. Shown in this figure are one suite of diffraction spots found in the c^* direction. The pictures have been normalized so that in each instance the distance in reciprocal space between the left-most and right-most spot is $4c_t^*$.

In Fig. 9, we have shown only an excerpt of the full diffraction images as we wish to illustrate most clearly the special features of chimney ladder diffraction patterns. As may be seen in this figure, we may associate with both the left-most diffraction spot and the right-most diffraction spot two additional series of diffraction spots. In the scheme shown at the bottom of Fig. 9, these two series are

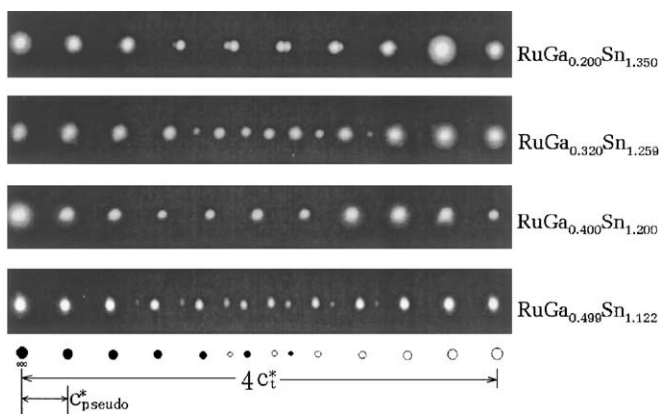

FIG. 9. Extracts of the electron diffraction micrographs. All samples are viewed down the [1 1 0] direction.

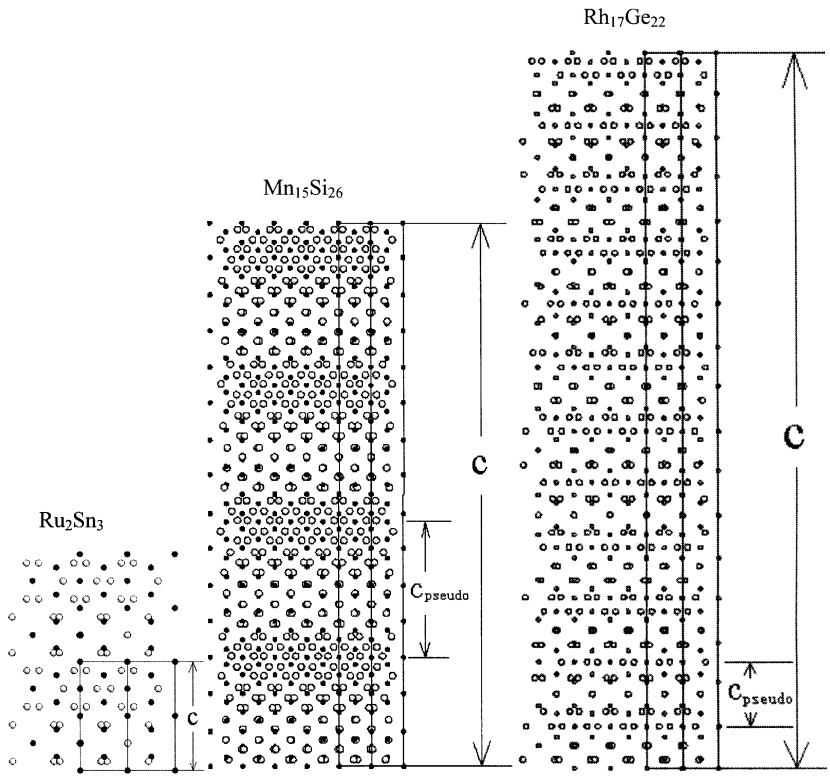

FIG. 10. The structures of Ru_2Sn_3, $Mn_{15}Si_{26}$, and $Rh_{17}Ge_{22}$, illustrating the relation between the true c axis and c_{pseudo}.

distinguished from one another by drawing the former sequence as filled circles and the latter sequence as open circles. In both the series of filled circles and the sequence of open circles, adjacent diffraction spots are equidistant from one another. We call this constant distance c^*_{pseudo}.

It may be seen that for $RuGa_{0.200}Sn_{1.350}$, $RuGa_{0.320}Sn_{1.260}$, and $RuGa_{0.499}Sn_{1.122}$ these two series do not overlap one another. In the case of $RuGa_{0.400}Sn_{1.200}$ they do. These results are typical of chimney ladder phases in general. The source of this overall pattern has been determined (40, 41).

It is most easily explained by examining Fig. 10, where we have illustrated the three chimney ladder phases Ru_2Sn_3, $Mn_{15}Si_{26}$, and $Rh_{17}Ge_{22}$ viewed down the [110] direction. As may be seen in this figure, in addition to the true c axis, one sees both for $Mn_{15}Si_{26}$ and for $Rh_{17}Ge_{22}$, the presence of a pseudo-axis, c_{pseudo}. In the case of $Mn_{15}Si_{26}$ $c_{pseudo} = \frac{1}{4}c$; for $Rh_{17}Ge_{22}$ $c_{pseudo} = \frac{1}{12}c$.

An examination of all 14-electron chimney ladder phases whose structures have been determined shows that there is a relation between the ratio c/c_{pseudo} and the stoichiometry of the T_tM_m phase (where t and m are integers). In general $c/c_{pseudo} = 2t - m$. Thus for $Mn_{15}Si_{26}$, $2t - m = (2 \times 15) - 26 = 4$, while for $Rh_{17}Ge_{22}$, $2t - m = (2 \times 17) - 22 = 12$. In the case of Ru_2Sn_3, no c_{pseudo} is visible as $2t - m = (2 \times 2) - 3 = 1$ and hence $c_{pseudo} = c$.

We may apply this general structural principle in accounting for the patterns seen in Fig. 9. It is easiest to do so in the case of $RuGa_{0.400}Sn_{1.200}$. Expressing this stoichiometry so that the numbers of atoms are integers, this compound is $Ru_5Ga_2Sn_6$. Therefore $c/c_{pseudo} = (2 \times 5) - 8 = 2$ and $c_t = c/t = c/5$. Equivalently, $c^*_{pseudo} = 2c^*$ and $5c^*$. We therefore find $c^*_t = 5/2\ c^*_{pseudo}$. As in Fig. 9, where the left-most and right-most spots are separated by a distance of 4 c^*_t, we expect to see ten regularly spaced spots in this interval, each separated by c^*_{pseudo} (as $4c^*_t = 4 \times 5/2\ c^*_{pseudo} = 10\ c^*_{pseudo}$). This is the experimentally observed pattern.

For the other systems illustrated in Fig. 10, the ratio of c^*_{pseudo}/c^*_t is more complex and hence more complex patterns are observed. From the results in Fig. 9, we may directly measure the ratio of c^*_t and c^*_{pseudo} and thus measure the ratio of t to $2t - m$. These values can be used to reconfirm the values of t and m determined by X-ray powder diffraction. In Table 3 we directly compare these two. We show the final tabulated results for micrographs taken normal to both the [110] and to [120] directions. It can be seen that the agreement between electron and powder diffraction data is good. Some deviations do exist. As powder diffraction is a more accurate method to determine cell axes, greater credence shall be given to values derived from this method.

TABLE 3
Refined Values of $t/(2t-m)$

Loaded stoichiometry	Powder indexation	Electron diffraction		
		[110] direction	[120] direction	Average
$RuGa_{0.200}Sn_{1.350}$	1.550	1.552	1.552	1.552
$RuGa_{0.320}Sn_{1.260}$	1.579	1.585	1.582	1.584
$RuGa_{0.400}Sn_{1.200}$	1.600	1.600	1.600	1.600
$RuGa_{0.499}Sn_{1.122}$	1.625	1.626	1.621	1.624

CONCLUSION

The ruthenium-gallium-stannide chimney ladder phases, like other previously known chimney ladder phases, continue to intrigue the examiner. In these systems there is a fairly invariant β-Sn transition metal sublattice, which is filled with a continuously varying array of main group atoms. The analogy can be made to the spring inside a jack-in-the box. The inner spring (i.e., the main group atoms) can be varied in length, but for any length it coils in a smooth fashion into the interior of the box (i.e., the transition metal lattice).

The source for the stability of these phases appears to be electronic in origin. This paper certainly further demonstrates the importance of the 14 electrons per transition metal rule. On the other hand, even though the data suggest that the ruthenium-gallium-stannide phases form as a solid solution, we cannot help but observe the parallel between this phase and other matter occupancy wave systems where electron concentration is known to be a dominant factor (6).

Here our attention turns to the γ-brass structure (6, 42, 43). In the γ-brass family there are two well-characterized structure types. First there is γ-brass itself, which is a cubic structure. Ni_2Zn_{11} adopts this type (44). Related to this cubic structure is the $NiZn_3$ structure, an orthorhombic variant (45). Of particular interest is γ-brass itself viewed down the [1 1 0] direction and the $NiZn_3$ structure seen down the [0 0 1] direction. In the former case, the structure reduces to parallel chains of atoms where five atoms of one chain correspond in length to three atoms of the other chain. In the latter case, the same type of pattern is observed but where the ratio is 13 to 8. These ratios are related to the Fibonacci sequence in a manner previously described for the ruthenium-gallium-stannide system. Also it is intriguing that γ-brass, like the chimney ladder phases, adopts a fixed electron concentration rule. This coincidence suggests the possibility that for certain MOW systems, specific ratios of sublattice lengths are preferred, and thus solid solutions need not form in the most exact manner.

ACKNOWLEDGMENTS

Financial support for this research from NSFC-29928001, the State Key Basic Research Program, and NSF-DMR-0073587 is gratefully acknowledged.

REFERENCES

1. J. A. Wilson, F. J. Disalvo, and S. Mahajan, *Adv. Phys.* **24,** 117 (1975).
2. P. Monceau, N. P. Ong, A. M. Portis, A. M. Meerschaut, and J. Rouxel, *Phys. Rev. Lett.* **37,** 602 (1976).
3. E. Canadell and M. H. Whangbo, *Chem. Rev.* **91,** 965 (1991).
4. B. G. Hyde and S. Andersson, "Inorganic Crystal Structures," pp. 305–329. Wiley, New York, 1989.
5. A. Yamamoto, *Acta Crystallogr. Sect. A* **49,** 831 (1993).
6. One of the best examples of MOW where electronic factors are important are the Hume-Rothery γ-brass structures. See W. Hume-Rothery, and G. V. Raynor, "The Structure of Metals and Alloys." Institute Of Metals, London, 1962.
7. O. Schwomma, A. Preisinger, H. Nowotny, and A. Wittmann, *Monatsh. Chem.* **95,** 1527 (1964).
8. O Schwomma, H. Nowotny, and A. Wittmann, *Monatsh. Chem.* **95,** 1538 (1964).
9. H. Völlenkle, A. Wittmann, and H. Nowotny, *Monatsh. Chem.* **95,** 1544 (1964).
10. H. Völlenkle, A. Wittmann, and H. Nowotny, *Monatsh. Chem.* **97,** 506 (1966).
11. H. Völlenkle, A. Preisinger, H. Nowotny, and A. Wittmann, *Z. Kristallogr.* **124,** 9 (1967).
12. G. Flieher, H. Völlenkle, and H. Nowotny, *Monatsh. Chem.* **98,** 2173 (1967).
13. H. Völlenkle, A. Wittmann, and H. Nowotny, *Monatsh. Chem.* **98,** 176 (1967).
14. G. Flieher, H. Völlenkle, and H. Nowotny, *Monatsh. Chem.* **99,** 877 (1968).
15. G. Flieher, H. Völlenkle, and H. Nowotny, *Monatsh. Chem.* **99,** 2408 (1968).
16. G. Zwilling and H. Nowotny, *Monatsh. Chem.* **102,** 672 (1971).
17. G. Zwilling and H. Nowotny, *Monatsh. Chem.* **104,** 668 (1973).
18. W. Jeitschko and E. Parthé, *Acta Crystallogr.* **22,** 417 (1967).
19. W. Jeitschko, *Acta Crystallogr. Sect. B* **33,** 2347 (1977).
20. V. I. Larchev and S.V. Popova, *J. Less-Common Met.* **84,** 87 (1982).
21. H. Takizawa, T. Sato, T. Endo, and M. Shimada, *J. Solid State Chem.* **73,** 427 (1988).
22. H. Takizawa, T. Sato, T. Endo, and M. Shimada, *J. Solid State Chem.* **68,** 234 (1987).
23. H. W. Knott, M. H. Mueller, and L. Heaton, *Acta Crystallogr.* **23,** 549 (1967).
24. F. E. Rohrer, H. Lind, L. Eriksson, A.-K. Larsson, and S. Lidin, *Z. Kristallogr.* **215,** 650 (2000).
25. D. J. Poutcharovsky and E. Parthé, *Acta Crystallogr. Sect. B* **30,** 2692 (1974).
26. F. E. Rohrer, H. Lind, L. Eriksson, A.-K. Larsson, and S. Lidin, *Z. Kristallogr.*, in press.
27. C. P. Susz, J. Muller, K. Yvon, and E. Parthé, *J. Less-Common Met.* **71,** 1 (1980).
28. W. B. Pearson, *Acta Crystallogr. Sect. B* **26,** 1044 (1970).
29. S. Okada, K. Kudou, M. Miyamoto, Y. Hikichi, and T. Lundström, *Chem. Soc. Jpn.* **7,** 701 (1992).
30. T. Kojima, I. Nishida, and T. Sakata, *J. Cryst. Growth* **47,** 589 (1979).
31. U. Gottlieb, O. Laborde, A. Rouault, and R. Madar, *Appl. Surf. Sci.* **73,** 243 (1993).

32. J. Evers, G. Oehlinger, and H. Meyer, *Mater. Res. Bull.* **19,** 1177 (1984).
33. M. Springborg, and R. Fischer, *J. Phys.: Condens. Matter* **10,** 701 (1998).
34. Yu. B. Kuz'ma and V. V. Milyan, *Inorg. Mat.* **15,** 11 (1979).
35. H. Nowotny, F. Benesovsky, and C. Brukl, *Monatsh. Chem.* **92,** 193 (1961).
36. H. Nowotny, *Prog. Solid State Chem.* **5,** 27 (1971).
37. D. Cheng, *J. Appl. Crystallogr.* **32,** 838 (1999).
38. K. Yvon, W. Jeitschko, and E. Parthé, *J. Appl. Cryst.* **10,** 73 (1997).
39. C. Janot, "Quasi-crystals: A Primer," 2nd ed. Oxford Univ. Press, New York, 1997.
40. R. De Ridder and S. Amelinckx, *Mater. Res. Bull.* **6,** 1223 (1971).
41. H. Q. Ye and S. Amelinckx, *J. Solid State Chem.* **61,** 8 (1986).
42. A. Morton, *Phys. Status Solidi A* **44,** 205 (1977).
43. S. Lee and L. Hoistad, *J. Alloys Comp.* **229,** 66 (1995).
44. A. Johansson, H. Ljung, and S. Westman, *Acta Chem. Scand.* **22,** 2743 (1968).
45. G. Novers and K. Schubert, *J. Less-Common Metals* **75,** 51 (1980).